

# Influence of wavelength and accumulated fluence at picosecond laser-induced surface roughening of copper on secondary electron yield

Cite as: J. Appl. Phys. **133**, 035303 (2023); <https://doi.org/10.1063/5.0131916>

Submitted: 25 October 2022 • Accepted: 28 December 2022 • Published Online: 19 January 2023

 Elena Bez,  Marcel Himmerlich,  Pierre Lorenz, et al.



View Online



Export Citation



CrossMark

## ARTICLES YOU MAY BE INTERESTED IN

[In-plane thermal conductivity measurements of Si thin films under a uniaxial tensile strain](#)  
Journal of Applied Physics **133**, 035103 (2023); <https://doi.org/10.1063/5.0125422>

[Bulk single crystals and physical properties of  \$\beta\$ -\(Al<sub>x</sub>Ga<sub>1-x</sub>\)<sub>2</sub>O<sub>3</sub> \(x=0-0.35\) grown by the Czochralski method](#)

Journal of Applied Physics **133**, 035702 (2023); <https://doi.org/10.1063/5.0131285>

[Crystal structure and site preference, magnetic and elastic properties, and martensitic transformation of Ni- and Fe-doped Co<sub>2</sub>VGa alloys: A first-principles study](#)

Journal of Applied Physics **133**, 035105 (2023); <https://doi.org/10.1063/5.0133379>

Journal of Applied Physics **Special Topics** Open for Submissions [Learn More](#)











# Influence of wavelength and accumulated fluence at picosecond laser-induced surface roughening of copper on secondary electron yield

Cite as: J. Appl. Phys. 133, 035303 (2023); doi: 10.1063/5.0131916

Submitted: 25 October 2022 · Accepted: 28 December 2022 ·

Published Online: 19 January 2023



Elena Bez,<sup>1,2,a)</sup>  Marcel Himmerlich,<sup>1</sup>  Pierre Lorenz,<sup>3</sup>  Martin Ehrhardt,<sup>3</sup>  Aidan Graham Gunn,<sup>1</sup>   
Stephan Pfeiffer,<sup>1</sup>  Martino Rimoldi,<sup>1</sup>  Mauro Tadorelli,<sup>1</sup> Klaus Zimmer,<sup>3</sup>  Paolo Chiggiato,<sup>1</sup>   
and André Anders<sup>2,3</sup> 

## AFFILIATIONS

<sup>1</sup>CERN (European Organization for Nuclear Research), 1211 Geneva 23, Switzerland

<sup>2</sup>Faculty of Physics and Earth Sciences, University of Leipzig, Linnéstraße 5, 04103 Leipzig, Germany

<sup>3</sup>Leibniz Institute of Surface Engineering (IOM), Permoserstraße 15, 04318 Leipzig, Germany

<sup>a)</sup>Author to whom correspondence should be addressed: [elena.annelie.bez@cern.ch](mailto:elena.annelie.bez@cern.ch)

## ABSTRACT

Ultrashort-pulse laser processing of copper is performed in air to reduce the secondary electron yield (SEY). By UV (355 nm), green (532 nm), and IR (1064 nm) laser-light induced surface modification, this study investigates the influence of the most relevant experimental parameters, such as laser power, scanning speed, and scanning line distance (represented as accumulated fluence) on the ablation depth, surface oxidation, topography, and ultimately on the SEY. Increasing the accumulated laser fluence results in a gradual change from a Cu<sub>2</sub>O to a CuO-dominated surface with deeper micrometer trenches, higher density of redeposited surface particles from the plasma phase, and a reduced SEY. While the surface modifications are less pronounced for IR radiation at low accumulated fluence (<1000 J/cm<sup>2</sup>), analogous results are obtained for all wavelengths when reaching the nonlinear absorption regime, for which the SEY maximum converges to 0.7. Furthermore, independent of the extent of the structural transformations, an electron-induced surface conditioning at 250 eV allows a reduction of the SEY maximum below unity at doses of 5×10<sup>-4</sup> C/mm<sup>2</sup>. Consequently, optimization of processing parameters for application in particle accelerators can be obtained for a sufficiently low SEY at controlled ablation depth and surface particle density, which are factors that limit the surface impedance and the applicability of the material processing for ultrahigh vacuum systems. The relations between processing parameters and surface features will provide guidance in treating the surface of vacuum components, especially beam screens of selected magnets of the Large Hadron Collider or of future colliders.

© 2023 Author(s). All article content, except where otherwise noted, is licensed under a Creative Commons Attribution (CC BY) license (<http://creativecommons.org/licenses/by/4.0/>). <https://doi.org/10.1063/5.0131916>

## I. INTRODUCTION

The buildup of electron clouds is a known performance limitation in hadron particle accelerators. Their formation is linked to the generation of secondary electrons that are multiplied when accelerated by the beam potential and impinge on the vacuum chamber walls. As a consequence, a pressure rise in the vacuum chamber, beam instabilities, and heat loads to the cryogenic system may occur.<sup>1-6</sup> At CERN, the high-luminosity upgrade of the Large Hadron Collider (HL-LHC)<sup>7,8</sup> envisages electron-cloud mitigation strategies for some specific parts of the machine: the inner surfaces

of beam screens—those surrounding the proton beam—require physical or chemical treatments to avoid electron multipacting, and ideally, the secondary electron yield (SEY)  $\delta$ —the ratio of the number of electrons emitted from the surface per incident electron—shall be reduced to below 1.1–1.3.<sup>9,10</sup> In a complex vacuum system, such as the one of the LHC, many limitations exist. For example, the surface roughness shall not exceed 25  $\mu\text{m}$  to ensure a low impedance at an operation temperature (5–20 K) of the 75  $\mu\text{m}$  thick Cu layer at the surface of the LHC beam screens. Furthermore, the method must be applicable *in situ* to some beam

screens already installed in LHC magnets and capable of processing their complete inner surface at a length up to 15 m. In terms of efficiency, the treatment must be reasonably fast; a campaign for treatment of one magnet should last no more than 1–2 months. CERN's current baseline strategy is to coat the surfaces of selected accelerator sections with amorphous carbon films.<sup>11,12</sup> The coating is based on DC magnetron sputtering and has been successfully applied in a series of magnets of the super proton synchrotron (SPS)<sup>13</sup> and in a standalone superconducting magnet of the LHC. Nevertheless, laboratory tests indicate that applying the coating to a fraction of the vacuum chamber sections, those that are equipped with fibrous cryosorbers, would less efficiently lower the SEY. Therefore, an alternative method is currently being studied.

Introducing surface roughness of tri- or rectangular-shaped grooves results in SEY reduction. In particular, a high aspect ratio of rectangular grooves or steep walls of triangular grooves efficiently traps secondary electrons.<sup>14</sup> Such structures are generated by laser beam scanning upon a surface. The formation process starts with material ablation, followed by an expanding plasma plume, and finishes with the partial redeposition of the nanoparticles ejected in the ablation process. The surface texture can be tailored to obtain specific surface properties by the choice of laser parameters. First treatments for electron-cloud mitigation in particle accelerators were performed on copper, aluminum, and stainless steel using an ns-pulsed laser.<sup>15</sup> Later, the impact of varying the laser parameters at wavelengths of 355 nm and 1064 nm<sup>16,17</sup> on the surface was investigated. However, optimization efforts have mainly been made on copper at a laser wavelength of 532 nm to further reduce the SEY. Thus, the laser pulse duration was shortened to 10 ps, the beam diameter was scaled down to reach higher fluences, and different scanning patterns were employed.<sup>18</sup> In this way, the SEY could be reduced to unity or even below in laboratory-scale experiments. In 2017, a successful first test of electron-cloud mitigation within a particle accelerator experiment was reported.<sup>18</sup> Recently, faster scanning resulted in a lower aspect ratio of the surface structures, implying an increased SEY. By varying the laser parameters, the aspect ratio of the trenches can be controlled. Even more important, the SEY reduction is dominated by the nanostructure and not only by the aspect ratio.<sup>19</sup> The presence of these loosely bound nanostructures is, however, of concern in beam pipes of a particle accelerator since they may randomly detach from the surface and interact with the proton beam. Additionally, the ablated material can deposit on the laser optics and reduce the light intensity in the interaction zone. Therefore, surface structures with reduced particle density are of special interest for application in particle accelerators, such as laser-induced periodic surface structures (LIPSS).<sup>20–23</sup> With this respect, the shallower groove depth and the applicability of faster scanning speeds are beneficial, despite reducing the SEY less efficiently. First treatments within the scope of electron-cloud mitigation showed SEY maxima in the range of 1.6 and 1.7.<sup>24,25</sup>

Here, the ablation depth and the SEY dependency on the accumulated laser fluence for three different wavelengths (355 nm, 532 nm, and 1064 nm) are explored. The topography and chemical composition of the processed surface are characterized and linked to these properties. Comparing three different wavelengths allows one to draw conclusions on ablation and SEY reduction efficiency

by considering practical constraints, such as the feasibility of guiding ultrashort laser pulses through a 15 m long fiber.

## II. EXPERIMENTAL DETAILS

For all treatments,  $2 \times 2 \text{ cm}^2$  Oxygen Free Electronic grade (OFE), flat copper samples were used. Before laser processing, the CERN standard procedure for UHV cleaning—which comprises wet-chemically degreasing with a commercial detergent and subsequent rinsing in de-ionized water—was applied to all samples. A Nd:YVO<sub>4</sub> pulsed laser was used as a photon source with a fixed pulse duration ( $\Delta t_p = 12 \text{ ps}$ ) and a repetition rate ( $f_{\text{rep}} = 100 \text{ kHz}$ ). The primary (1064 nm), doubled (532 nm), and tripled (355 nm) laser frequencies were employed. Laser processing in air was performed varying the average laser power  $P$  and the scanning speed  $v$  from 10 mW up to 4100 mW and from 1 to 200 mm/s, respectively. The linearly polarized Gaussian beam (with a quality factor  $M^2 < 1.3$ ) was focused by a f-theta lens with focal lengths of 165 (IR and green) and 103 mm (UV) on the surface and scanned in parallel lines with distances  $\Delta y$  of 10 and 50  $\mu\text{m}$ . The laser spot diameters  $d$  were determined following Liu's method<sup>26</sup> and were evaluated to be 26.4 (IR), 11.6 (green), and 29.2  $\mu\text{m}$  (UV), respectively.

Furthermore, all given accumulated laser fluences  $F$  refer to the accumulated energy  $E$  per surface area and are calculated by the following equation:

$$F = \frac{E \cdot f_{\text{rep}}}{v \Delta y} = \frac{P}{v \Delta y} \quad (\text{J}/\text{cm}^2). \quad (1)$$

This averaged quantity cannot be generally used for comparison of effects, but it allows us to follow processing trends within defined parameter limits. For the ps-laser operating at 100 kHz, it is a useful value if the scanned lines neither overlap too much nor are too far separated ( $d/2 < \Delta y < 10 \cdot d$ ). In the case of a stronger overlap, the line distance  $\Delta y$  should be replaced by the laser diameter in Eq. (1).

A commercial ultrahigh vacuum (UHV) system, with a base pressure below  $2 \times 10^{-10}$  mbar (SPECS Surface Nano Analysis GmbH, Berlin, Germany), is used for SEY and XPS characterization of the processed samples. The system consists of a hemispherical electron energy analyzer with 9 channeltrons (Phoibos 150) and a monochromated AlK $\alpha$  x-ray source (XR50M,  $h\nu = 1486.7 \text{ eV}$ ). The energy scale of the analyzer is regularly calibrated using sputter-cleaned polycrystalline Cu, Ag, and Au foils. For the analysis of the secondary electron yield between 50 and 1800 eV primary electron energy, an electron beam of  $\sim 2 \text{ nA}$  generated by a Kimball Physics ELG-2 electron gun at a distance of 2 cm from the sample was focused to a spot diameter of 1 mm on the surface. The details of the setup and the implemented experimental conditions are described in Ref. 27, a sample bias of  $\pm 47.1 \text{ V}$  was used, and the sample current was measured using an optical isolation amplifier with a gain of  $10^8 \text{ V/A}$  in combination with a 6517B electrometer (Keithley Instruments, Inc., Cleveland, USA). The influence of electron irradiation on the SEY (*conditioning*) on the laser-processed surfaces was investigated in a second UHV setup (base pressure of  $2 \times 10^{-10}$  mbar). The system comprises two electron sources: a flood

gun (FG15/40 SPECS Surface Nano Analysis GmbH, Berlin, Germany) that irradiates the surface at an electron energy of 250 eV and a second electron source (Kimball Physics ELG-2 electron gun) to carry out the SEY measurement after exposure to defined electron doses. The SEY is measured via a positively biased collector (+45 V), while the sample is kept at a negative bias (−18 V).<sup>11</sup> The surface topography was characterized by field emission scanning electron microscopy (FE-SEM) using a ZEISS Sigma and ZEISS Gemini Ultra 55 system.

After the surface analyses, the samples were embedded in a transparent resin and mechanically ground on a silicon carbide paper, and then polished using a diamond water based solution. Once the cross section had been dissected, the maximum ablation depth defined as the distance between the surface of the untreated regions and the groove valley (see Fig. 1) was measured using a digital optical microscope (Keyence VHX-6000).

### III. RESULTS AND DISCUSSION

The raster scanning of the laser spot across the surface generates a pattern of parallel grooves. The depth of the grooves extracted from the cross-sectional profiles (Fig. 1—selected examples) strongly depends on the laser parameters used. The laser wavelength ( $\lambda = 532$  nm), the line distance ( $\Delta y = 50$   $\mu\text{m}$ ), and the scanning speed ( $v = 1$  mm/s) were constant, while the average laser power was varied. Within these parameter settings, the measured ablation depth is ranging from 7 up to 91  $\mu\text{m}$  for the highest average laser power. Structures that are only a few micrometers deep are difficult to observe with this method (the lower measurement limit is  $\sim 4$   $\mu\text{m}$ ). According to Fig. 1, a higher average laser power leads to

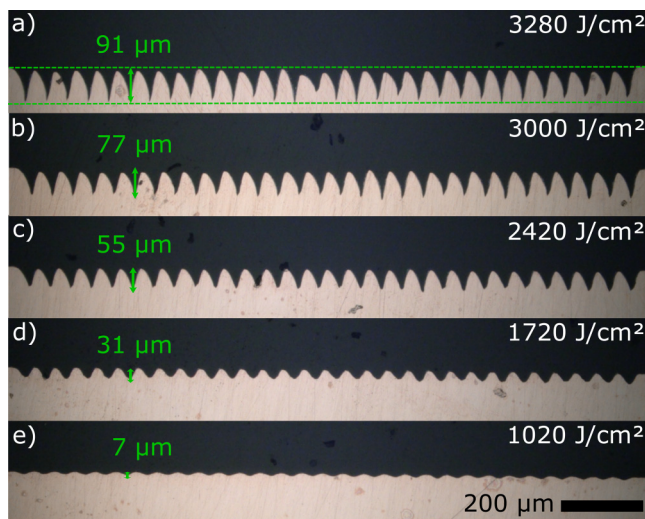


**FIG. 1.** Cross sections of selected laser-treated samples:  $\lambda = 532$  nm, line distance  $\Delta y = 50$   $\mu\text{m}$ , scanning speed  $v = 1$  mm/s, and average laser powers of (a) 1640, (b) 1500, (c) 1210, (d) 860, and (e) 510 mW. The maximum ablation depth is measured from the surface of the untreated regions to the valley of the deepest trenches as illustrated by the two dashed lines in (a).

removal of more material and, thus, to deeper grooves, an expected tendency according to previous studies.<sup>19,28</sup> The cross sections of a wide data set of UV, green, and IR irradiated surfaces at a fixed line distance ( $\Delta y = 10$   $\mu\text{m}$ ) were measured, and the ablation depth was found to increase with accumulated laser fluence for all three wavelengths (Fig. 2). While the ablation depth for green and IR laser light roughly matches each other, UV irradiation (blue dots) results in about 50 % deeper grooves at similar fluences. When comparing these numbers, it has to be considered that the  $2.5\times$  smaller focus of the green laser created only a slight overlap of the raster-scanned lines, whereas UV and IR scanned lines overlapped by more than 10  $\mu\text{m}$ . The laser diameter is, however, not considered in the definition of the accumulated fluence. The determination of the maximum ablation depth is relevant since it must be less than 25  $\mu\text{m}$ . The LHC beam screens consist of a 75  $\mu\text{m}$  thick copper layer laminated onto stainless steel, which must not be completely penetrated by the laser, because the impedance of the copper layer increases if the generated surface structures are too deep and perpendicularly aligned to the proton beam propagation direction in the LHC.<sup>29</sup> Otherwise, the image current that travels with the proton beams at the beam screen inner surface can induce too high heat loads to the surrounding cryogenic system.

The typical primary electron energy ( $E_p$ ) dependence of the SEY for flat Cu OFE that underwent surface decreasing exhibits a maximum SEY ( $\delta_{\text{max}}$ ) at  $E_p \sim 250$  eV between 1.8 and 2.2, variability ascribed to the “aging” of the sample.<sup>27,30</sup> Figure 3 shows  $\delta(E_p)$  after laser treatment at accumulated fluences ranging from 65 to 4500  $\text{J}/\text{cm}^2$  and employing the three different laser wavelengths. The curves indicate that the SEY was reduced to 1.2 and below at a primary electron energy of 250 eV. Concomitantly, the maximum

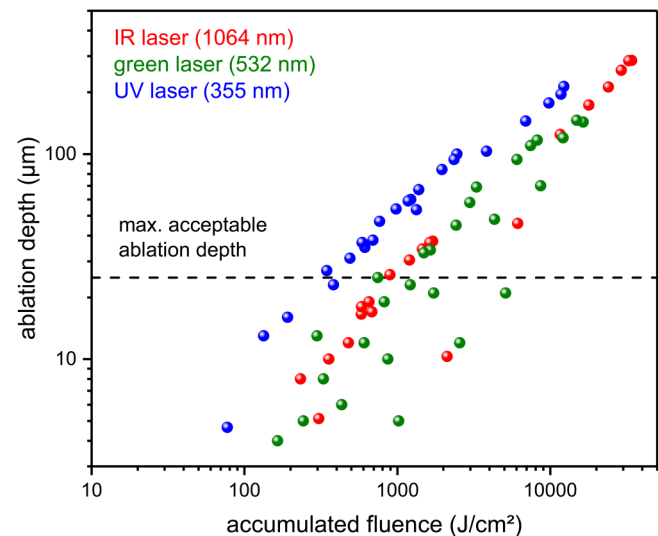


**FIG. 2.** Measured ablation depths in dependence of accumulated fluence at a line distance of 10  $\mu\text{m}$  for IR (red dots), green (green), and UV (blue) laser irradiation. The maximum acceptable ablation depth is indicated with the dashed line at 25  $\mu\text{m}$ . Please note the double-logarithmic scale—equivalent plots in a linear scale can be found in the [supplementary material](#).



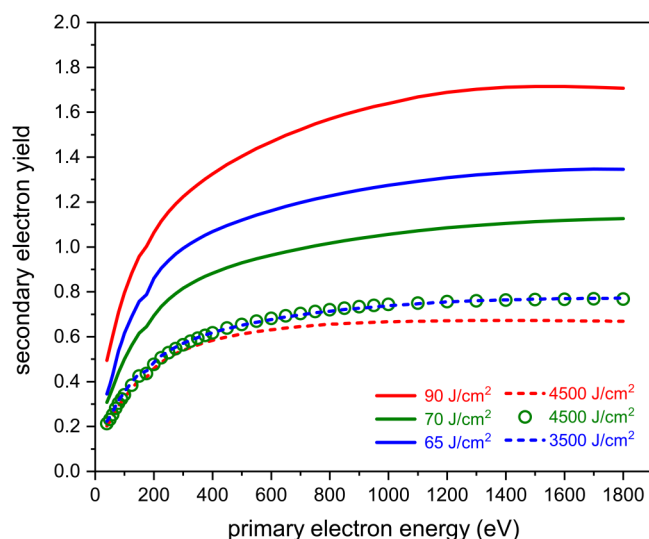


**FIG. 3.** SEY in dependence of primary electron energy of laser-irradiated copper samples using wavelengths of 355 (blue), 532 (green), and 1064 nm (red). The actual accumulated fluence is indicated in the legend, and the corresponding scanning electron micrographs are shown on the right side of Fig. 4.

$E(\delta_{\max})$  shifts to higher energies (between 1200 and 1800 eV) and exceeds, especially for low fluences, the SEY values of degreased Cu at these electron energies. The electrons, which contribute to multipacting in the LHC vacuum pipe, have energies up to 500 eV,<sup>31</sup> and the data clearly show that the laser treatment efficiently reduces the SEY in this range (Fig. 3) via the creation of a grooved surface and

the coverage with nanoparticles (Fig. 4, right). On a microscopic scale, primary electrons impinge obliquely on the inclined surface regions. As a consequence, forward scattering and trapping of electrons in the formed structures contribute to the effective reduction of the number of electrons that are emitted.

The SEY maxima of a larger variety of samples follow a general decrease with increasing accumulated fluence for all three laser wavelengths (Fig. 4). Two regimes can be identified: for low fluences ( $<1000$  J/cm<sup>2</sup>), the SEY maximum is affected by the wavelength, being the highest for 1064 nm, and varies with accumulated fluence. For  $F \geq 1000$  J/cm<sup>2</sup>, the three curves converge to  $\delta_{\max} = 0.7$ , the lowest value achieved in the experiments reported here. The change in SEY with accumulated fluence is linked to variations in the topography and the chemical composition of the surface. Generally, the morphology of the processed samples consists of the already analyzed grooves (Fig. 1), decorated with nanometer-sized features. In the high fluence range ( $F \geq 1000$  J/cm<sup>2</sup>), the surfaces are covered by a compact layer of nanoparticles in a cauliflower-shaped arrangement that originates from the redeposition of ablated particles (Fig. 4, right—bottom row). The sample irradiated with green laser light, however, exhibits more spherical particles than the others.

Due to the reduced laser fluence, the surfaces formed at  $F \sim 100$  J/cm<sup>2</sup> are characterized by a low ablation depth (Fig. 2) as well as low density of surface particles (Fig. 4, right—top row). Under these conditions, UV or IR laser irradiation results in spherical structures of different size and density, originating from resolidified Cu that was molten during laser interaction, while the green light creates ripples, which resemble laser-induced periodic surface structures (LIPSS) and are decorated by nanospheres. A representative comparison of the different surface features in dependence of fluence, average laser power, and scan speed for the

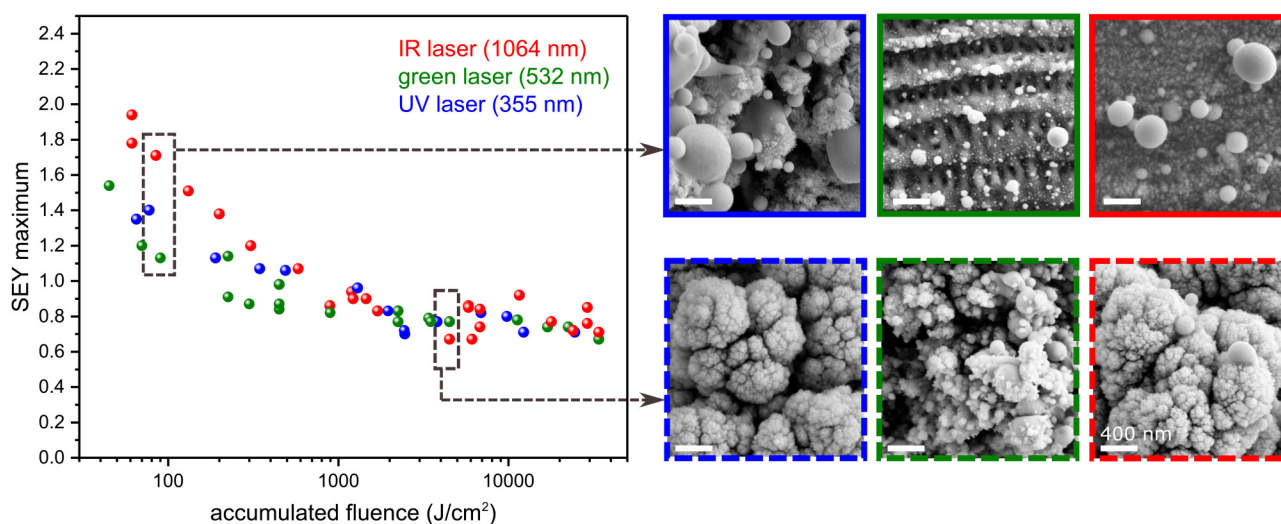


**FIG. 4.** Left: SEY maximum in dependence of the accumulated fluence for UV (355 nm), green (532 nm), and IR (1064 nm) picosecond laser pulses. Right: scanning electron micrographs of selected samples that had been created at low (top row) and high (bottom row) accumulated laser fluence (indicated by the dashed boxes, the corresponding SEY curves are shown in Fig. 3). The white scale bars in the micrographs correspond to a length of 400 nm.

example of UV as well as IR irradiation can be found elsewhere.<sup>32,33</sup> The structures described in these earlier studies show a similar tendency at a gradual variation from low to high fluence.

The processes at the surface and in the plasma plume as well as the resulting chemical reactions have been found dependent on the ambient conditions during laser ablation.<sup>34</sup> The present study concentrates on evaluating laser processes performed in ambient air, where oxidation is not suppressed. To characterize the influence of the laser irradiation on the composition of the copper surface, XPS measurements were performed for selected samples after exposure to light pulses of different wavelengths and varying the accumulated fluence. Detailed XPS analyses of untreated copper surfaces were reported elsewhere.<sup>35</sup> A gradual change of the surface composition is found in the Cu<sub>2</sub>p<sub>3/2</sub> and Cu LMM spectra (Fig. 5). For fluences higher than 2000 J/cm<sup>2</sup>, for which the SEY saturated at a low level around 0.7–0.8, the Cu<sub>2</sub>p<sub>3/2</sub> and O1s core level binding energy is 933.7 and 529.6 eV, respectively, and the kinetic energy of the Cu LMM Auger transition is 917.7 eV, which is equivalent to an Auger parameter of 1851.4 eV. The shape of the Cu spectra resembles those of CuO.<sup>36–38</sup> The corresponding peak energies of samples irradiated with very low *F* on the other hand are at 932.4, 530.3, and 916.8 eV, respectively, leading to an Auger parameter of 1849.2 eV. In this case, the surface is predominantly Cu<sub>2</sub>O.<sup>38–40</sup> In addition, surface adsorbates, such as hydrocarbon species as well as oxygen-containing molecules, are present at

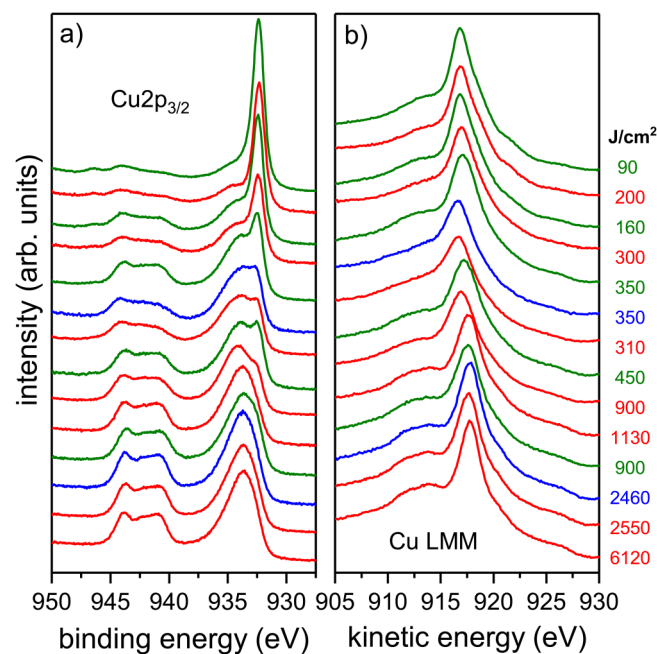


**FIG. 5.** X-ray photoelectron spectra: (a) Cu<sub>2</sub>p<sub>3/2</sub> state and (b) Cu LMM x-ray excited Auger emission of selected samples that were laser-treated with different accumulated fluence (as indicated in the legend on the right) and wavelength (color-coded, red lines, and numbers are used if the sample was irradiated by 1064 nm laser light, green values correspond to samples treated using 532 nm, and blue is equivalent to processing with 355 nm photons).

the surface with distinct features, such as a shoulder around 531.4–531.5 eV in the O1s state (supplementary material). In the transition region of intermediate fluence, there is also an indication of copper hydroxide surface species, detected in the Cu<sub>2</sub>p<sub>3/2</sub> spectrum at 934.3 eV and by a slight shift of the LMM Auger line of Cu.

A gradual transition from pure CuO for very high laser fluence via the coexistence of CuO and Cu<sub>2</sub>O for the intermediate region to a Cu<sub>2</sub>O-dominated surface for very low fluence is evident from the XPS spectra series (Fig. 5). In correlation with the changes in surface topography, this behavior can be explained considering the laser light–matter interaction. When exposing a metallic surface to femto- or picosecond laser pulses, the photon energy is absorbed by the material via inverse Bremsstrahlung or photoionization. In contrast to nanosecond laser processing, a thermal non-equilibrium between the heated electrons and the cold lattice is created during the laser pulse. The energy transfer to the lattice starts on a time scale of picoseconds due to electron–phonon coupling and heat conduction, described in the two-temperature-model.<sup>41,42</sup> Material can be removed by Coulomb explosion<sup>43</sup> at lower laser intensities or by thermal vaporization, and trenches in the shape of the laser beam are created. The interaction of the laser beam with the evaporated material forms an expanding plasma. This plasma plume interacts with the ambient air, decouples a shock wave, and eventually confines. After electron–ion recombination, particles and clusters are ejected from the plume, partially redeposited onto the surface so that nanostructures are created.<sup>44,45</sup> For the implemented experimental conditions, accumulated fluences of  $F \geq 1000$  J/cm<sup>2</sup> lead to a high number of redeposited CuO nanoparticles, which most likely form in the plasma plume and are oxidized due to the oxygen-containing environment. An additional process, particles formed from the melt in the course of laser plasma–target interactions, may also be applicable, though its relative importance cannot be judged from the data available.

As the XPS and SEY data indicate, there exists a saturation fluence around 2000 J/cm<sup>2</sup> for which neither a further increment of the CuO content at the surface nor a further reduction of the SEY (Fig. 4) can be obtained when increasing *F*. This behavior may be attributed to two phenomena. First, at high accumulated fluence, which is comparable to a slow scanning speed during the processing, the number of pulses per surface area increases to such an extent that the self-limitation of the laser pulses becomes relevant (i.e., the plasma plume resulting from the previous pulse might not have yet fully decayed as the next pulse strikes). As a result, the remaining particle vapor and/or plasma can shield the laser intensity so that only a fraction of its intensity reaches the target surface. In addition, with higher power, the electron density of the expanding plasma plume increases, making it more opaque as the laser radiation is absorbed via inverse Bremsstrahlung, photo-ionization, or other absorption mechanisms.<sup>46</sup> As a consequence, the ablation rate is normally limited due to plasma shielding.<sup>47,48</sup> However, in our study, the ablation depth did not fully saturate for very high fluences (Fig. 2), but a slope decrease was observed (supplementary material). Considering the SEY trend vs the accumulated fluence (Fig. 4) at high fluence, a conclusion is that very deep trenches do not add a significant benefit for SEY reduction, as the electrons hardly reach these regions. Second, the SEM images of samples

processed at high fluence reveal a high density of nanoparticles that cover the whole surface. The surface capacity of trapping redeposited particles might be limited causing further particles not adhering anymore. These effects can also explain that an ultimate low SEY limit for all three wavelengths exists and highlight the role of the surface nanoparticle layer on the SEY reduction. It is important to further highlight that the ultimate low SEY was not provoked by the presence of CuO. For comparison: a non-structured CuO surface has a higher SEY than non-structured Cu<sub>2</sub>O. CuO is not required to achieve very low SEY as processing in nitrogen atmosphere, where the formation of CuO is suppressed, results in similarly low values.<sup>34</sup> In addition, CuO-dominated surfaces are not particularly favored for applications in particle accelerators as they can lead to surface charging at cryogenic temperature and inferior SEY reduction upon electron irradiation.<sup>49</sup>

A gradual decrease of  $F$  from 1000 to 100 J/cm<sup>2</sup> reduces the density of redeposited particles, which is directly observed by microscopy and indirectly traceable by the decreasing contribution of CuO-related contributions to the Cu2p<sub>3/2</sub> XPS spectrum. This gradual change of surface properties is translated to an increase of the SEY. Finally, at very low fluence, the ablation threshold<sup>19</sup> of the materials plays an important role. In this case, the surface topography can still transform, but neither strong removal nor redeposition of material will occur. The laser irradiation modifies the surface composition only slightly, as a fairly low amount of surface hydroxide and hydrocarbon adsorbates are found.

As a general trend, at low fluences ( $F \leq 1000$  J/cm<sup>2</sup>), the performance of the IR laser light for surface structuring and SEY reduction is worse, which is reflected by the tendencies in Figs. 3 and 4. Due to the higher efficiency at a shorter wavelength,<sup>50</sup> a higher fluence of IR light is needed to obtain the same surface composition found for green or UV-processed surfaces. Explanations for this behavior can be partially given by the absorbance of the material, while the reflectivity  $R$  of a smooth copper surface at room temperature is below 50% for 355 and 532 nm and  $R \geq 90\%$  at 1064 nm. Therefore, for low fluences (implying a low number of laser pulses or low average laser power), only a small fraction of the laser pulse energy is absorbed by the material in the infrared range.

Regarding the requirements that are essential for the *in situ* laser processing of LHC beam screens, a comparison of Figs. 2 and 4 is important. At the maximum acceptable ablation depth of 25  $\mu$ m, the accumulated fluence is 900 J/cm<sup>2</sup> (IR), 750 J/cm<sup>2</sup> (green), and 380 J/cm<sup>2</sup> (UV), respectively. The corresponding SEY maxima at those fluences are 0.85 (IR), 0.8 (green), and 1 (UV). These are the maximum fluences that can be applied to obtain SEY  $\leq 1$  and an ablation depth below 25  $\mu$ m. The lower limit is defined at the fluence where  $\delta_{\max} = 1$ , namely, 650 J/cm<sup>2</sup> (IR), 130 J/cm<sup>2</sup> (green), and 380 J/cm<sup>2</sup> (UV). For these lower limits, the processing time amounts to 95 s/cm<sup>2</sup> (UV), 32.5 s/cm<sup>2</sup> (green), and 162.5 s/cm<sup>2</sup> (IR) at an average laser power of 4 W. Hence, all three laser wavelengths meet the requirements, but the acceptable fluence range of the green laser is the widest and the processing time the lowest. Furthermore, even though UV processing is very efficient in material removal, it seems disadvantageous regarding the preservation of the copper layer on the beam screen surface due to the relatively high ablation depth. The setup, which is currently foreseen for *in*

*situ* laser processing of beam screens up to 15 m in length, includes a sufficiently long optical fiber<sup>51</sup> and a laser-fiber coupling system, combined with an inchworm robot. For green and, particularly, for IR laser light, technological solutions exist to transmit high-power ps pulses through a fiber, whereas such solutions are lacking for UV light.

Finally, as an important factor for the characterization and qualification of the surface processing, the change of SEY was evaluated when the surfaces are exposed to an electron beam. This conditioning test is intended to model the self-limited variation of the surface properties via electron-cloud buildup in scrubbing runs of particle accelerators<sup>52,53</sup> and during their continuous operation.<sup>54</sup> When a flat air-exposed Cu surface is exposed to electrons, adsorbed molecules are removed by electron-stimulated desorption and chemical surface reactions are induced, such as the graphitization of hydrocarbon adsorbates as well as dissociation of surface hydroxides, resulting in a reduction of the SEY.<sup>27,55</sup> Selected laser-processed samples with an initial SEY maximum varying between 0.8 and 1.8 were irradiated by 250 eV electrons to investigate how they condition upon a stepwise increase of the electron dose. The observed variation of  $\delta_{\max}$  up to a dose of approximately  $3 \times 10^{-2}$  C/mm<sup>2</sup> (Fig. 6) proves that there is, in all cases, a clear conditioning effect due to changes of the surface properties:<sup>27</sup> generally, the lower the initial  $\delta_{\max}$ , the lower the final value after conditioning. Samples with an initial value below 1.6 condition to below 1, whereas the one with the initial SEY maximum higher than 1.6 remains above 1, even at electron doses  $> 10^{-2}$  C/mm<sup>2</sup>.

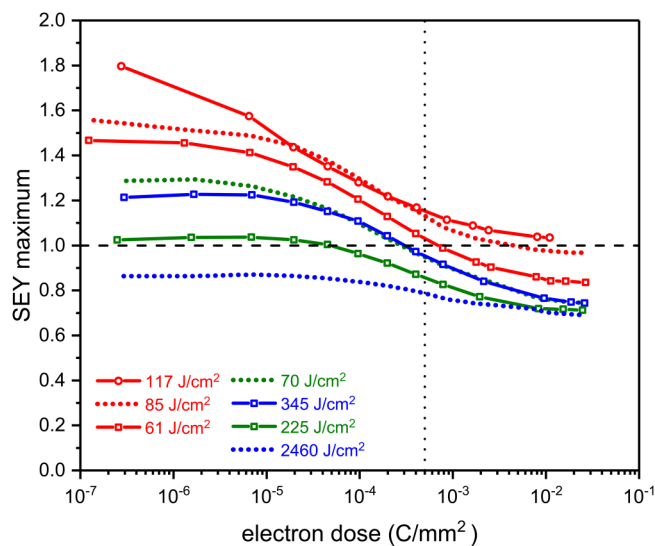


**FIG. 6.** Variation of the SEY maximum in dependence of the electron dose during conditioning of 355 (blue), 532 (green), and 1064 nm (red) laser-irradiated samples processed with different accumulated fluences (as indicated in the legend) and with different initial SEY maxima. The dashed horizontal line indicates a SEY of 1, and the dotted vertical line refers to an electron dose of  $5 \times 10^{-4}$  C/mm<sup>2</sup>.

These tendencies allow us to engineer the laser treatment process for efficient electron-cloud mitigation via optimization between very low SEY on one hand and reduction of surface particle density, ablation depth, and increase of processing speed on the other hand. This result gives us more flexibility in choosing the laser processing parameters as well as the laser wavelength. The accumulated fluence range, in which the processed surface fulfills the constraints regarding the SEY maximum and the ablation depth, can be extended to lower values. Processing at lower fluence is beneficial as the ablation depth is much smaller (Fig. 2), the surfaces are less oxidized (Fig. 5), and covered by fewer particles (Fig. 4). Considering the electron conditioning results (Fig. 6) and the technical constraints for scrubbing campaigns, a good compromise for acceptable conditioning performance in applications for accelerators can be found when targeting a treatment that creates a surface with an initial  $\delta_{\max}$  of 1.4–1.5 that reaches values below unity at electron doses  $\leq 5 \times 10^{-4}$  C/mm<sup>2</sup>.

#### IV. CONCLUSIONS

The influence of wavelength, covering the range from UV to IR, and accumulated fluence on the structuring of copper via 12 ps laser irradiation at a 100 kHz repetition rate was investigated to study the correlation to SEY reduction. The surface structures were characterized regarding the resulting ablation depth, the formed surface morphology, the secondary electron yield, the chemical composition in dependence on the average laser power, the scanning speed, and the line distance at a given focal spot size. Independent of the laser wavelength, two clear relations were found. First, the ablation depth increases with increasing laser fluence. Second, the resulting SEY maximum is reduced for increasing accumulated fluence to an ultimate limit of 0.7. Comparing the three laser wavelengths, UV and green laser irradiation is more efficient for processes at low laser fluence than IR with respect to SEY reduction. However, when overcoming a certain accumulated laser fluence, similar SEY and surface morphologies are obtained. The results verify that a  $\delta_{\max} \leq 1$  can be achieved for ablation depths not larger than 25  $\mu\text{m}$  for all three wavelengths, which is an important constraint for aspects of surface impedance in the application of the processed Cu on surfaces of LHC beam screens. For the intended *in situ* processing of LHC magnet beam screens with a length of up to 15 m, fast scanning speed and low density of surface particles are targeted. All three laser wavelengths allow the optimization of the processing parameters accordingly with a clear correlation found between the accumulated laser fluence and the resulting surface topography and composition, both directly influencing the secondary electron emission. The SEY can be gradually reduced when increasing the laser fluence. Electron conditioning is also efficient for laser-structured Cu samples and allows us to define a trade-off between the antithetical physical and technical requirements. Noteworthy, irradiation by the green laser provides the lowest SEY at an acceptable ablation depth, while in terms of low-cost and reliability of the processing system, an infrared laser may be a reasonable alternative considering the technical requirement of transmitting the high-power light pulses through a long fiber.

#### SUPPLEMENTARY MATERIAL

See the [supplementary material](#) for details on Figs. 2 and 5.

#### ACKNOWLEDGMENTS

The support by the Wolfgang Gentner Programme of the German Federal Ministry of Education and Research (Grant No. 13E18CHA) for the Ph.D. scholarship of E. Bez is gratefully acknowledged.

#### AUTHOR DECLARATIONS

##### Conflict of Interest

The authors have no conflicts to disclose.

##### Author Contributions

**Elena Bez:** Conceptualization (equal); Formal analysis (equal); Investigation (equal); Methodology (equal); Visualization (lead); Writing – original draft (lead). **Marcel Himmerlich:** Conceptualization (equal); Formal analysis (equal); Investigation (equal); Project administration (equal); Supervision (lead); Visualization (supporting); Writing – original draft (supporting); Writing – review & editing (equal). **Pierre Lorenz:** Formal analysis (equal); Methodology (equal); Project administration (equal); Resources (lead). **Martin Ehrhardt:** Methodology (equal); Resources (equal). **Aidan Graham Gunn:** Formal analysis (equal); Investigation (equal); Writing – review & editing (equal). **Stephan Pfeiffer:** Formal analysis (equal); Investigation (equal); Writing – review & editing (equal). **Martino Rimoldi:** Formal analysis (equal); Investigation (equal); Writing – review & editing (equal). **Mauro Taborelli:** Project administration (equal); Supervision (supporting); Writing – review & editing (equal). **Klaus Zimmer:** Project administration (equal); Supervision (supporting); Writing – review & editing (equal). **Paolo Chiggiato:** Funding acquisition (lead); Writing – review & editing (equal). **André Anders:** Supervision (supporting); Writing – review & editing (equal).

#### DATA AVAILABILITY

The data that support the findings of this study are available from the corresponding author upon reasonable request.

#### REFERENCES

- <sup>1</sup>R. Cimino and T. Demma, “Electron cloud in accelerators,” *Int. J. Mod. Phys. A* **29**, 1430023 (2014).
- <sup>2</sup>F. Zimmermann, “Review of single bunch instabilities driven by an electron cloud,” *Phys. Rev. ST Accel. Beams* **7**, 124801 (2004).
- <sup>3</sup>G. Rumolo, F. Ruggiero, and F. Zimmermann, “Simulation of the electron-cloud build up and its consequences on heat load, beam stability, and diagnostics,” *Phys. Rev. ST Accel. Beams* **4**, 012801 (2001).
- <sup>4</sup>G. Iadarola, B. Bradu, P. Dijkstal, L. Mether, G. Rumolo, G. Skripka, and L. Taviani, “Overview on heat loads in the LHC,” in *Proceedings of the Joint INFN-CERN-ARIES Workshop on Electron-Cloud Effects 2018, Elba, Italy* (CERN, 2020), pp. 51–58.
- <sup>5</sup>G. Rumolo, H. Bartosik, E. Belli, G. Iadarola, K. Li, L. Mether, A. Romano, F. Zimmermann, P. Dijkstal, and M. Schenk, “Electron cloud effects at the CERN accelerators,” in *Proceedings of the Joint INFN-CERN-ARIES Workshop on Electron-Cloud Effects 2018, Elba, Italy* (CERN, 2020), pp. 13–20.



- <sup>6</sup>G. Skripka, P. Dijkstal, G. Iadarola, L. Mether, G. Rumolo, and E. Wulff, "Comparison of electron cloud build-up simulations against heat load measurements for the LHC arcs with different beam configurations," in *Proceedings of IPAC'19* (JACoW Publishing, 2019), pp. 3232–3235.
- <sup>7</sup>G. Apollinari, I. Béjar Alonso, O. Brüning, P. Fessia, M. Lamont, L. Rossi, and L. Tavian, *High-Luminosity Large Hadron Collider (HL-LHC): Technical Design Report V. 0.1*, CERN Yellow Reports: Monographs (CERN, 2017). <http://cds.cern.ch/record/1567014/files/p9.pdf>.
- <sup>8</sup>G. Arduini, J. Barranco, A. Bertarelli, N. Biancacci, R. Bruce, O. Brüning, X. Buffat, Y. Cai, L. Carver, S. Fartoukh, M. Giovannozzi, G. Iadarola, K. Li, A. Lechner, L. M. Medrano, E. Métral, Y. Nosochkov, Y. Papaphilippou, D. Pellegrini, T. Pieloni, J. Qiang, S. Redaelli, A. Romano, L. Rossi, G. Rumolo, B. Salvant, M. Schenck, C. Tambasco, R. Tomás, S. Valishev, and F. V. der Veken, "High luminosity LHC: Challenges and plans," *J. Instrum.* **11**, C12081 (2016).
- <sup>9</sup>G. Iadarola and G. Rumolo, "Electron cloud in the CERN accelerators (PS, SPS, LHC)," (2013).
- <sup>10</sup>G. Iadarola, "Electron cloud studies for CERN particle accelerators and simulation code development," Ph.D. thesis (CERN, 2014). <http://cds.cern.ch/record/1603635/files/p19.pdf>.
- <sup>11</sup>P. Costa Pinto, S. Calatroni, H. Neupert, D. Letant-Delrieux, P. Edwards, P. Chiggiato, M. Taborelli, W. Vollenberg, C. Yin-Vallgren, J. Colaax, and S. Lucas, "Carbon coatings with low secondary electron yield," *Vacuum* **98**, 29–36 (2013).
- <sup>12</sup>C. Yin Vallgren, G. Arduini, J. Bauche, S. Calatroni, P. Chiggiato, K. Cornelis, P. C. Pinto, B. Henrist, E. Métral, H. Neupert, G. Rumolo, E. Shaposhnikova, and M. Taborelli, "Amorphous carbon coatings for the mitigation of electron cloud in the CERN super proton synchrotron," *Phys. Rev. ST Accel. Beams* **14**, 071001 (2011).
- <sup>13</sup>W. Vollenberg, P. Chiggiato, P. Costa Pinto, P. Cruikshank, H. Moreno, C. Pasquino, J. Perez Espinos, and M. Taborelli, "Amorphous carbon coating in SPS," in *Proceedings of IPAC'21* (JACoW Publishing, 2021), pp. 3475–3478.
- <sup>14</sup>M. Pivi, F. K. King, R. E. Kirby, T. O. Raubenheimer, G. Stupakov, and F. Le Pimpec, "Sharp reduction of the secondary electron emission yield from grooved surfaces," *J. Appl. Phys.* **104**, 104904 (2008).
- <sup>15</sup>R. Valizadeh, O. B. Malyshev, S. Wang, S. A. Zolotovskaya, W. A. Gillespie, and A. Abdolvand, "Low secondary electron yield engineered surface for electron cloud mitigation," *Appl. Phys. Lett.* **105**, 231605 (2014).
- <sup>16</sup>R. Valizadeh, O. B. Malyshev, and S. Wang, "Low secondary electron yield of laser treated surfaces of copper, aluminum and stainless steel," in *Proceedings of IPAC'16* (JACoW, 2016), pp. 1089–1092.
- <sup>17</sup>R. Valizadeh, O. B. Malyshev, S. Wang, T. Sian, M. D. Cropper, and N. Sykes, "Reduction of secondary electron yield for e-cloud mitigation by laser ablation surface engineering," *Appl. Surf. Sci.* **404**, 370–379 (2017).
- <sup>18</sup>S. Calatroni, E. Garcia-Tabares Valdivieso, H. Neupert, V. Nistor, A. T. Perez Fontenla, M. Taborelli, P. Chiggiato, O. Malyshev, R. Valizadeh, S. Wackerow, S. A. Zolotovskaya, W. A. Gillespie, and A. Abdolvand, "First accelerator test of vacuum components with laser-engineered surfaces for electron-cloud mitigation," *Phys. Rev. Accel. Beams* **20**, 113201 (2017).
- <sup>19</sup>D. Bajek, S. Wackerow, D. A. Zanin, L. Baudin, K. Bogdanowicz, E. G.-T. Valdivieso, S. Calatroni, B. Di Girolamo, M. Sitko, M. Himmerlich, M. Taborelli, P. Chiggiato, and A. Abdolvand, "Role of surface microgeometries on electron escape probability and secondary electron yield of metal surfaces," *Sci. Rep.* **10**, 250 (2020).
- <sup>20</sup>M. Birnbaum, "Semiconductor surface damage produced by ruby lasers," *J. Appl. Phys.* **36**, 3688–3689 (1965).
- <sup>21</sup>J. Bonse, S. Höhm, S. V. Kirner, A. Rosenfeld, and J. Krüger, "Laser-induced periodic surface structures—A scientific evergreen," *IEEE J. Sel. Top. Quantum Electron.* **23**, 9000615 (2017).
- <sup>22</sup>J. Bonse and S. Gräf, "Maxwell meets Marangoni—A review of theories on laser-induced periodic surface structures," *Laser Photonics Rev.* **14**, 2000215 (2020).
- <sup>23</sup>J. Long, P. Fan, M. Zhong, H. Zhang, Y. Xie, and C. Lin, "Superhydrophobic and colorful copper surfaces fabricated by picosecond laser induced periodic nanostructures," *Appl. Surf. Sci.* **311**, 461–467 (2014).
- <sup>24</sup>R. Valizadeh, O. B. Malyshev, T. Sian, J. S. Colligon, Q. Li, and W. Perrie, "Laser ablated surface engineering: From discovery to machine application," in *Proceedings of the Joint INFN-CERN-ARIES Workshop on Electron-Cloud Effects 29018, Elba, Italy* (CERN, 2020), pp. 209–216.
- <sup>25</sup>J. J. Nivas, M. Valadan, M. Salvatore, R. Fittipaldi, M. Himmerlich, M. Rimoldi, A. Passarelli, E. Allahyari, S. L. Oscurato, A. Vecchione, C. Altucci, S. Amoroso, A. Andreone, S. Calatroni, and M. R. Masullo, "Secondary electron yield reduction by femtosecond pulse laser-induced periodic surface structuring," *Surf. Interfaces* **25**, 101179 (2021).
- <sup>26</sup>J. M. Liu, "Simple technique for measurements of pulsed Gaussian-beam spot sizes," *Opt. Lett.* **7**, 196–198 (1982).
- <sup>27</sup>V. Petit, M. Taborelli, H. Neupert, P. Chiggiato, and M. Belhaj, "Role of the different chemical components in the conditioning process of air exposed copper surfaces," *Phys. Rev. Accel. Beams* **22**, 083101 (2019).
- <sup>28</sup>S. Wang, Y. Ren, C. Cheng, J. Chen, and D. Tzou, "Micromachining of copper by femtosecond laser pulses," *Appl. Surf. Sci.* **265**, 302–308 (2013).
- <sup>29</sup>S. Calatroni, M. Arzeo, S. Aull, M. Himmerlich, P. Costa Pinto, W. Vollenberg, B. Di Girolamo, P. Cruikshank, P. Chiggiato, D. Bajek, S. Wackerow, and A. Abdolvand, "Cryogenic surface resistance of copper: Investigation of the impact of surface treatments for secondary electron yield reduction," *Phys. Rev. Accel. Beams* **22**, 063101 (2019).
- <sup>30</sup>R. Larciprete, D. R. Grosso, M. Comisso, R. Flammini, and R. Cimino, "Secondary electron yield of Cu technical surfaces: Dependence on electron irradiation," *Phys. Rev. ST Accel. Beams* **16**, 011002 (2013).
- <sup>31</sup>R. Cimino and I. Collins, "Vacuum chamber surface electronic properties influencing electron cloud phenomena," *Appl. Surf. Sci.* **235**, 231–235 (2004).
- <sup>32</sup>P. Lorenz, M. Himmerlich, M. Ehrhardt, E. Bez, K. Bogdanowicz, M. Taborelli, and K. Zimmer, "Secondary electron yield reduction of copper after 355 nm ultrashort pulse laser ablation," *Lasers Manuf. Mater. Process.* **9**, 135–150 (2022).
- <sup>33</sup>P. Lorenz, M. Himmerlich, M. Ehrhardt, E. Bez, K. Bogdanowicz, M. Taborelli, and K. Zimmer, "Secondary electron yield engineering of copper surfaces using ultra short infrared laser pulses," *Proc. SPIE* **11989**, 73–83 (2022).
- <sup>34</sup>S. Calatroni, E. Garcia-Tabares Valdivieso, A. T. Perez Fontenla, M. Taborelli, H. Neupert, M. Himmerlich, P. Chiggiato, D. Bajek, S. Wackerow, and A. Abdolvand, "Optimization of the secondary electron yield of laser-structured copper surfaces at room and cryogenic temperature," *Phys. Rev. Accel. Beams* **23**, 033101 (2020).
- <sup>35</sup>V. Petit, "Conditioning of surfaces in particle accelerators," Theses (Institut Supérieur de l'Aéronautique et de l'Espace, 2020). <https://hal.archives-ouvertes.fr/tel-02919120/file/DPHY20102.1597843660-4.pdf>.
- <sup>36</sup>J. Ghijsen, L. H. Tjeng, J. van Elp, H. Eskes, J. Westerink, G. A. Sawatzky, and M. T. Czyzyk, "Electronic structure of Cu<sub>2</sub>O and CuO," *Phys. Rev. B* **38**, 11322–11330 (1988).
- <sup>37</sup>T. Schedel-Niedrig, T. Neisius, I. Böttger, E. Kitzelmann, G. Weinberg, D. Demuth, and R. Schlögl, "Copper (sub)oxide formation: A surface sensitive characterization of model catalysts," *Phys. Chem. Chem. Phys.* **2**, 2407–2417 (2000).
- <sup>38</sup>M. C. Biesinger, "Advanced analysis of copper x-ray photoelectron spectra," *Surf. Interface Anal.* **49**, 1325–1334 (2017).
- <sup>39</sup>S. Poulston, P. M. Parlett, P. Stone, and M. Bowker, "Surface oxidation and reduction of CuO and Cu<sub>2</sub>O studied using XPS and XAES," *Surf. Interface Anal.* **24**, 811–820 (1996).
- <sup>40</sup>D. Tahir and S. Tougaard, "Electronic and optical properties of Cu, CuO and Cu<sub>2</sub>O studied by electron spectroscopy," *J. Condens. Matter Phys.* **24**, 175002 (2012).
- <sup>41</sup>S. I. Anisimov, B. L. Kapeliovich, and T. L. Perel'man, "Electron emission from the metal surfaces induced by ultrashort laser pulses," *J. Exp. Theor. Phys.* **39**, 375–377 (1974). <http://jetp.ras.ru/cgi-bin/e/index/e/39/2/p375?a=list>.
- <sup>42</sup>B. N. Chichkov, C. Momma, S. Nolte, F. von Alvensleben, and A. Tünnermann, "Femtosecond, picosecond and nanosecond laser ablation of solids," *Appl. Phys. A* **63**, 109–115 (1996).

- <sup>43</sup>R. Stoian, D. Ashkenasi, A. Rosenfeld, and E. E. B. Campbell, “Coulomb explosion in ultrashort pulsed laser ablation of  $\text{Al}_2\text{O}_3$ ,” *Phys. Rev. B* **62**, 13167–13173 (2000).
- <sup>44</sup>E. Gamaly and A. Rode, “Physics of ultra-short laser interaction with matter: From phonon excitation to ultimate transformations,” *Prog. Quantum. Electron.* **37**, 215–323 (2013).
- <sup>45</sup>D. Bäuerle, *Laser Processing and Chemistry* (Springer, Berlin, 2011).
- <sup>46</sup>S. S. Harilal, J. R. Freeman, P. K. Diwakar, and A. Hassanein, “Femtosecond laser ablation: Fundamentals and applications,” in *Laser-Induced Breakdown Spectroscopy: Theory and Applications* (Springer, Berlin, 2014), pp. 143–166.
- <sup>47</sup>D. Marla, U. V. Bhandarkar, and S. S. Joshi, “A model of laser ablation with temperature-dependent material properties, vaporization, phase explosion and plasma shielding,” *Appl. Phys. A* **116**, 273–285 (2014).
- <sup>48</sup>S. Tan, J. Wu, Y. Zhang, M. Wang, and Y. Ou, “A model of ultra-short pulsed laser ablation of metal with considering plasma shielding and non-Fourier effect,” *Energies* **11**, 3163 (2018).
- <sup>49</sup>V. Petit, M. Taborelli, D. A. Zanin, M. Himmerlich, H. Neupert, P. Chiggiato, and G. Iadarola, “Beam-induced surface modifications as a critical source of heat loads in the large hadron collider,” *Commun. Phys.* **4**, 192 (2021).
- <sup>50</sup>L. Tunna, A. Kearns, W. O’Neill, and C. Sutcliffe, “Micromachining of copper using Nd: YAG laser radiation at 1064, 532, and 355 nm wavelengths,” *Opt. Laser Technol.* **33**, 135–143 (2001).
- <sup>51</sup>M. Sitko, V. Baglin, S. Calatroni, P. Chiggiato, B. Di Girolamo, E. G. T. Valdivieso, M. Taborelli, A. Abdolvand, D. Bajek, S. Wackerow, and M. Colling, “Towards implementation of laser engineered surface structures for electron cloud mitigation,” in *Proceedings of 9th International Particle Accelerator Conference* (JACoW Publishing, 2018), pp. 1220–1223.
- <sup>52</sup>O. Bruning, F. Caspers, I. Collins, O. Grobner, B. Henrist, N. Hilleret, J.-M. Laurent, M. Morvillo, M. Pivi, F. Ruggiero, and X. Zhang, “Electron cloud and beam scrubbing in the LHC,” in *Proceedings of the 1999 Particle Accelerator Conference* (IEEE, 1999), pp. 2629–2631.
- <sup>53</sup>Y. Suetsugu, K. Shibata, T. Ishibashi, K. Kanazawa, M. Shirai, S. Terui, and H. Hisamatsu, “First commissioning of the SuperKEKB vacuum system,” *Phys. Rev. Accel. Beams* **19**, 121001 (2016).
- <sup>54</sup>E. Buratin, V. Baglin, B. Henrist, P. Chiggiato, and A. Fasoli, “Electron flux and pressure dynamic in the LHC vacuum pilot sector as a function of beam parameters and beam pipe properties,” *Phys. Rev. Accel. Beams* **23**, 114802 (2020).
- <sup>55</sup>R. Cimino, M. Comisso, D. R. Grosso, T. Demma, V. Baglin, R. Flammini, and R. Larciprete, “Nature of the decrease of the secondary-electron yield by electron bombardment and its energy dependence,” *Phys. Rev. Lett.* **109**, 064801 (2012).